

# Synthesis of Composite Films in Tb<sub>2</sub>O<sub>3</sub>–Al<sub>2</sub>O<sub>3</sub> Eutectic System by CVD Method and Their Tb<sup>3+</sup>-centered Luminescence

Natsumi Imai and Akihiko Ito\*

Graduate School of Environment and Information Sciences, Yokohama National University,  
79-7 Tokiwadai, Hodogaya-ku, Yokohama, Kanagawa 240-8501, Japan

(Received October 31, 2025; accepted December 22, 2025)

**Keywords:** Tb<sub>2</sub>O<sub>3</sub>–Al<sub>2</sub>O<sub>3</sub> eutectic system, composite, chemical vapor deposition, luminescence

Composite films in the Tb<sub>2</sub>O<sub>3</sub>–Al<sub>2</sub>O<sub>3</sub> eutectic system were synthesized on sapphire substrates by the laser-assisted chemical vapor deposition method. On a *c*-cut sapphire substrate, TbAlO<sub>3</sub> (TAP)– $\alpha$ -Al<sub>2</sub>O<sub>3</sub> and Tb<sub>3</sub>Al<sub>5</sub>O<sub>12</sub> (TAG)– $\alpha$ -Al<sub>2</sub>O<sub>3</sub> composite films were obtained at 6.4–39.6 mol%Tb<sub>2</sub>O<sub>3</sub> in precursor vapor. At compositions close to the eutectic point of 22.0 mol%Tb<sub>2</sub>O<sub>3</sub>, a lamellar structure formed, whereas at compositions far from the eutectic point, a rod-like structure formed. Both TAP– $\alpha$ -Al<sub>2</sub>O<sub>3</sub> and TAG– $\alpha$ -Al<sub>2</sub>O<sub>3</sub> composite films exhibited green luminescence originating from the <sup>5</sup>D<sub>4</sub>–<sup>7</sup>F<sub>*n*</sub> (*n* = 3–6) transitions of Tb<sup>3+</sup> centers with decay time constants of 0.67 and 1.46 ms for the TAP– $\alpha$ -Al<sub>2</sub>O<sub>3</sub> composite film and 0.75 and 1.31 ms for the TAG– $\alpha$ -Al<sub>2</sub>O<sub>3</sub> composite film.

## 1. Introduction

Directionally solidified eutectics are composite materials in which two or more solid phases precipitate simultaneously from the melt. Eutectics based on the  $\alpha$ -Al<sub>2</sub>O<sub>3</sub> phase have been studied since the 1990s as high-temperature structural materials for aerospace applications, owing to their excellent strength and thermal stability at high temperatures.<sup>(1–3)</sup> In the RE<sub>2</sub>O<sub>3</sub>–Al<sub>2</sub>O<sub>3</sub> eutectic system (RE = rare-earth element), REAP (rare-earth aluminum perovskite, REAlO<sub>3</sub>)– $\alpha$ -Al<sub>2</sub>O<sub>3</sub> eutectics were obtained for RE = Sm–Gd, Y, whereas REAG (rare-earth aluminum garnet, RE<sub>3</sub>Al<sub>5</sub>O<sub>12</sub>)– $\alpha$ -Al<sub>2</sub>O<sub>3</sub> eutectics were obtained for RE = Tb–Lu, Y.<sup>(4)</sup>

By introducing luminescent centers as dopants into REAG and REAP, eutectics can be applicable as phosphors. Ce<sup>3+</sup>-doped YAG exhibits yellow luminescence,<sup>(5)</sup> and thus, Ce<sup>3+</sup>-doped YAG– $\alpha$ -Al<sub>2</sub>O<sub>3</sub> eutectics excited by a blue LED has been studied for white LED application.<sup>(6,7)</sup> Structural advantages have also been reported for GAP– $\alpha$ -Al<sub>2</sub>O<sub>3</sub> eutectics, because emission light propagates within the matrix via total internal reflection, efficiently guiding scintillation light to the detector.<sup>(8–10)</sup> Reports on the synthesis of eutectics focusing on the Tb<sub>2</sub>O<sub>3</sub>– $\alpha$ -Al<sub>2</sub>O<sub>3</sub> eutectic are scarce, limited to research on Ce<sup>3+</sup>-doped Tb<sub>3</sub>Al<sub>5</sub>O<sub>12</sub> (TAG)– $\alpha$ -Al<sub>2</sub>O<sub>3</sub> eutectics for LED application.<sup>(11,12)</sup> Tb<sup>3+</sup> has been widely used as a dopant, whereas

---

\*Corresponding author: e-mail: [ito-akihiko-xr@ynu.ac.jp](mailto:ito-akihiko-xr@ynu.ac.jp)  
<https://doi.org/10.18494/SAM6091>

(TbAlO<sub>3</sub>) TAP and TAG contain Tb<sup>3+</sup> in their crystal structures and exhibit localized luminescence from Tb<sup>3+</sup> centers.

All these eutectics were synthesized via the melt-solidification process, which often resulted in an inhomogeneous, Chinese script-like microstructure.<sup>(13–15)</sup> Therefore, new process methods for forming ordered structures are required. Our research group focused on the CVD method, which enables film synthesis at low temperatures. However, conventional thermal CVD methods struggled to form composite films with a two-phase separation structure. By incorporating laser technology into thermal CVD, we have successfully formed composite films with phase-separated structures in pseudo-binary eutectic systems such as ZrO<sub>2</sub>–Al<sub>2</sub>O<sub>3</sub> and HfO<sub>2</sub>–Al<sub>2</sub>O<sub>3</sub>.<sup>(16,17)</sup> We have succeeded in synthesizing single-phase and composite films with phase-separated structures in YAG–Al<sub>2</sub>O<sub>3</sub> and LuAG–Al<sub>2</sub>O<sub>3</sub> systems.<sup>(18–20)</sup>

The present study extends the LCVD technique to the Tb<sub>2</sub>O<sub>3</sub>–Al<sub>2</sub>O<sub>3</sub> eutectic system. The objective is to analyze the constituent phases and microstructure of the obtained films and evaluate their luminescence properties.

## 2. Materials and Methods

The laser-assisted CVD apparatus has been described elsewhere.<sup>(21)</sup> The synthesis conditions follow those of previous studies on  $\alpha$ -Al<sub>2</sub>O<sub>3</sub>–REAG (RE = Lu, Y) composite films.<sup>(18,19)</sup> Metal-organic compounds of terbium tris(dipivaloylmethanate) (Strem Chemicals, USA) and aluminum tris(acetylacetonate) (Sigma-Aldrich, USA) were maintained at temperatures of 443–473 K and 453 K, respectively, in precursor furnaces. The resultant vapor was transferred to the CVD chamber using Ar as carrier gas, and O<sub>2</sub> gas was separately introduced to the chamber through a double-tubed nozzle. The molar ratios in the precursor vapor were estimated from the mass change in each precursor before and after deposition, and the molar ratios of Tb<sub>2</sub>O<sub>3</sub> were determined to be 6.4–39.6 mol%. The total chamber pressure was maintained at 230–250 Pa. The substrates were *m*-, *c*-, *a*-, and *r*-cut sapphire single crystals (5 × 5 × 0.5 mm<sup>3</sup>) polished on both sides. Each substrate was preheated on a heating stage, then irradiated with a CO<sub>2</sub> laser (wavelength: 10.6  $\mu$ m; maximum laser output: 60 W) through a ZnSe window. The laser irradiation heated all the substrates to 1000–1216 K. The deposition time was 600 s. The phase compositions of the resultant films were determined by X-ray diffraction (XRD; Bruker D2 Phaser, USA). The microstructures were observed by scanning electron microscopy (SEM; JEOL JCM-6000, Japan). The photoluminescence (PL) and PL excitation (PLE) spectra and afterglow decay curves were measured using a fluorescence spectrophotometer (JASCO FP-8300, Japan).

## 3. Results and Discussion

Figure 1 shows XRD patterns and photographs of composite films synthesized on a *c*-cut sapphire substrate. The films were translucent. The XRD patterns were indexed to the TAP (ICSD No. 98302), TAG (ICSD No. 33602), and  $\alpha$ -Al<sub>2</sub>O<sub>3</sub> (ICSD No. 130948) phases. Because only the diffraction peaks on the same plane as the substrate were measured for  $\alpha$ -Al<sub>2</sub>O<sub>3</sub>, the

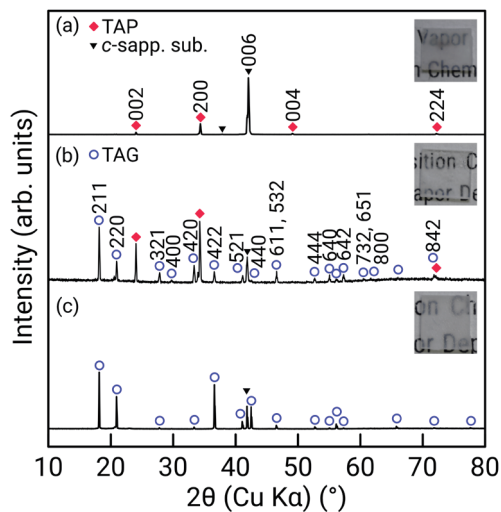


Fig. 1. (Color online) XRD patterns and photographs of the films prepared on *c*-cut sapphire substrate at various compositions: (a) 7.7, (b) 13.9, and (c) 27.0 mol% $\text{Tb}_2\text{O}_3$ .

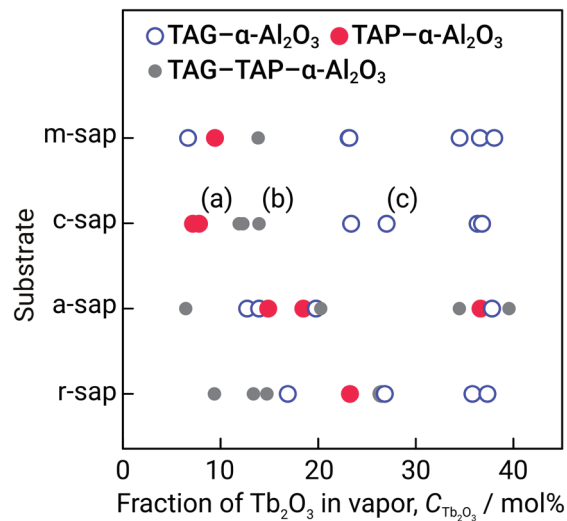


Fig. 2. (Color online) Phase mapping of the films prepared on *m*-, *c*-, *a*-, and *r*-cut sapphire substrates as a function of  $\text{Tb}_2\text{O}_3$  molar ratio in precursor vapor. (a), (b), and (c) correspond to the XRD patterns in Fig. 1.

$\alpha\text{-Al}_2\text{O}_3$  phase within the composite film exhibited homoepitaxial growth relative to the substrate. Figure 2 shows the phase mapping of the obtained films. The  $\text{TAP-}\alpha\text{-Al}_2\text{O}_3$  (filled circle) and  $\text{TAG-}\alpha\text{-Al}_2\text{O}_3$  (open circle) composite films tended to form on the Tb-poor and Tb-rich sides of the eutectic point (22.0 mol% $\text{Tb}_2\text{O}_3$ ), respectively. In some films, it was a three-phase mixed-phase film (gray-filled circle). Although the TAP and  $\alpha\text{-Al}_2\text{O}_3$  phases tended to form on the Al-rich side and the TAG and  $\alpha\text{-Al}_2\text{O}_3$  phases tended to form on the Tb-rich side, differences in the obtained phases on each plane of the sapphire substrate might be likely affected by differences between the composition in the precursor vapor and the composition within the film or by lattice matching between the substrate plane and each TAP and TAG phase.

Figure 3 shows SEM-BEI images of the composite films prepared on a *c*-cut sapphire substrate at various compositions. The light and dark gray areas correspond to the TAG or TAP phase and the  $\alpha\text{-Al}_2\text{O}_3$  phase, respectively. Composite films were formed in the range of 6.4–39.6 mol% $\text{Tb}_2\text{O}_3$ , with film thicknesses of 1.51–9.16  $\mu\text{m}$ . Deposition rates of the films were 9.1–55.0  $\mu\text{m h}^{-1}$ . Figure 4 shows the structural mapping of the composite films prepared on various substrates. At compositions close to the eutectic point of 22.0 mol% $\text{Tb}_2\text{O}_3$ , a lamellar structure formed (light- and dark-gray-filled squares in Fig. 4), while at compositions far from the eutectic point, a rod-like structure formed (open and filled squares in Fig. 4). On the Tb-poor side of the eutectic point, TAP and TAG were dispersed in the  $\alpha\text{-Al}_2\text{O}_3$  matrix, whereas on the Tb-rich side,  $\alpha\text{-Al}_2\text{O}_3$  was dispersed in the TAP and TAG matrix. Some films had a fine particulate dispersed structure formed within the grown grains (triangles in Fig. 4).

Figures 5(a) and 5(b) show the PLE and PL spectra of the  $\text{TAP-}\alpha\text{-Al}_2\text{O}_3$  and  $\text{TAG-}\alpha\text{-Al}_2\text{O}_3$  composite films prepared on a *c*-plane sapphire substrate at 7.7 and 27.0 mol% $\text{Tb}_2\text{O}_3$ ,

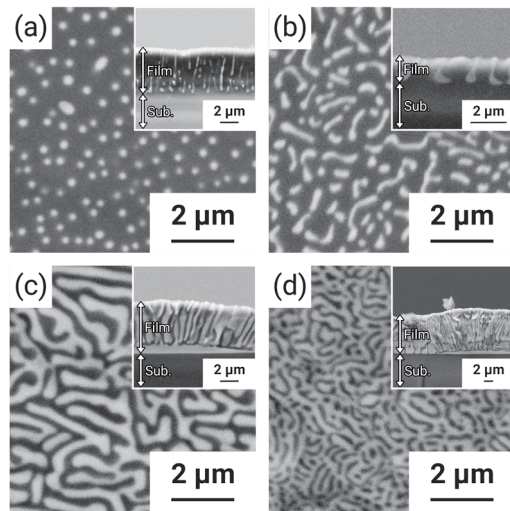


Fig. 3. Surface SEM-BEI images of the films prepared on *c*-cut sapphire substrate: (a) TAP- $\alpha$ -Al<sub>2</sub>O<sub>3</sub> film (7.7 mol% Tb<sub>2</sub>O<sub>3</sub>), (b) TAP-TAG- $\alpha$ -Al<sub>2</sub>O<sub>3</sub> film (13.9 mol% Tb<sub>2</sub>O<sub>3</sub>), (c) TAG- $\alpha$ -Al<sub>2</sub>O<sub>3</sub> film (27.0 mol% Tb<sub>2</sub>O<sub>3</sub>), and (d) TAG- $\alpha$ -Al<sub>2</sub>O<sub>3</sub> film (36.3 mol% Tb<sub>2</sub>O<sub>3</sub>). The light and dark areas correspond to the TAP or TAG phase and the  $\alpha$ -Al<sub>2</sub>O<sub>3</sub> phase, respectively. Insets show the corresponding cross-sectional images.

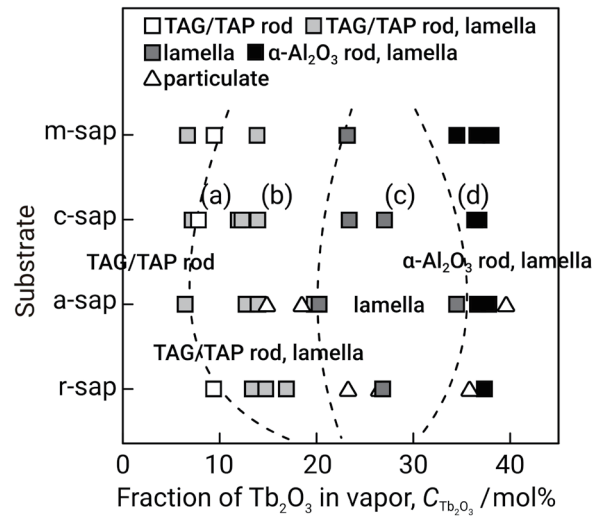


Fig. 4. Structural mapping of the films prepared on *m*-, *c*-, *a*-, and *r*-cut sapphire substrates as a function of Tb<sub>2</sub>O<sub>3</sub> molar ratio in precursor vapor: TAG/TAP rod in  $\alpha$ -Al<sub>2</sub>O<sub>3</sub> matrix (open square), TAG/TAP rod and lamella in  $\alpha$ -Al<sub>2</sub>O<sub>3</sub> matrix (light-gray-filled square), lamella (dark-gray-filled square),  $\alpha$ -Al<sub>2</sub>O<sub>3</sub> rod and lamella in TAG/TAP matrix (filled matrix), and particulate dispersed structure (triangle). (a)–(d) correspond to the SEM images in Fig. 3.

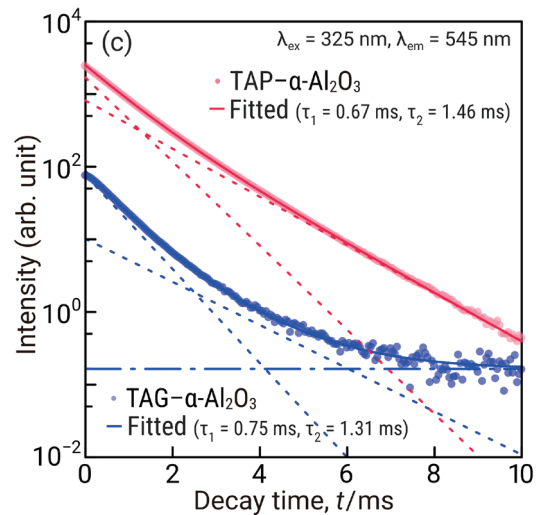
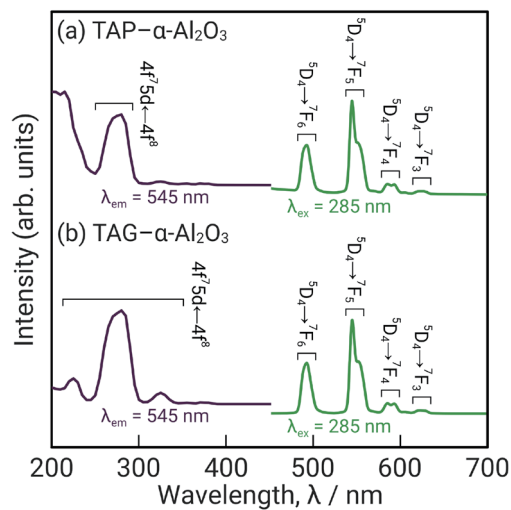


Fig. 5. (Color online) PLE spectrum monitored at 545 nm and PL spectrum excited at 325 nm for (a) TAP- $\alpha$ -Al<sub>2</sub>O<sub>3</sub> composite film prepared on *c*-cut sapphire substrate at 7.7 mol% Tb<sub>2</sub>O<sub>3</sub> and (b) TAG- $\alpha$ -Al<sub>2</sub>O<sub>3</sub> composite film prepared on *c*-cut sapphire substrate at 27.0 mol% Tb<sub>2</sub>O<sub>3</sub>. (c) Afterglow decay profiles monitored at 545 nm and excited at 325 nm of the corresponding TAP- and TAG- $\alpha$ -Al<sub>2</sub>O<sub>3</sub> composite films. Solid lines indicate the total fitting curves with bi-component exponential function.

respectively. The PLE peaks in the wavelength range of 200–350 nm were attributed to the transition of the  $4f^8$  level to the  $4f^75d$  level of  $Tb^{3+}$  centers in the TAP, TAG, and  $\alpha-Al_2O_3$  phases.<sup>(22–24)</sup> The PLE absorption at 230 nm was prominent for  $Tb^{3+}$  in the  $\alpha-Al_2O_3$  phase, suggesting that  $Tb^{3+}$  was solid-solved in the  $\alpha-Al_2O_3$  phase of the TAP- $\alpha-Al_2O_3$  films. The PL peaks in the wavelength range of 450–650 nm were associated with the transition of the  $^5D_4$  level to the  $^7F_n$  ( $n = 3–6$ ) levels of  $Tb^{3+}$  centers in the TAP, TAG, and  $\alpha-Al_2O_3$  phases.<sup>(23–27)</sup> The PL spectra were nearly identical regardless of the substrate plane and microstructure. This might be because the peak position of the f-f transition of  $Tb^{3+}$  is less susceptible to the effect of the coordination environment. Figure 5(c) shows the afterglow decay curves of the corresponding TAP- $\alpha-Al_2O_3$  and TAG- $\alpha-Al_2O_3$  composite films measured at 545 nm and excited at 325 nm. The measured decay curves were fitted with a bi-component exponential function:

$$I(t) = A_1 \exp(-t/\tau_1) + A_2 \exp(-t/\tau_2) + C, \quad (1)$$

where  $t$  is the decay time,  $A_1$  and  $A_2$  are constants,  $\tau_1$  and  $\tau_2$  are decay time constants, and  $C$  is a constant for baseline (if needed).  $\tau_1$  and  $\tau_2$  were determined to be 0.67 and 1.46 ms for the TAP- $\alpha-Al_2O_3$  composite film and 0.75 and 1.31 ms for the TAG- $\alpha-Al_2O_3$  composite film, respectively, using the Fityk software.<sup>(28)</sup>

Onishi *et al.* studied the decay curves of  $Tb^{3+}$  in the TAP, TAG, and  $\alpha-Al_2O_3$  phases measured at 545 nm with a tri-component exponential function, and they reported that the decay time constants were 0.0039, 0.02, and 0.53 ms for the  $Tb^{3+}$  center in the TAP phase,<sup>(22)</sup> 0.02, 0.1, and 1.3 ms for the  $Tb^{3+}$  center in the TAG phase,<sup>(23)</sup> and 0.06, 0.40, and 1.43 ms for the  $Tb^{3+}$  center in the  $\alpha-Al_2O_3$  phase.<sup>(24)</sup> Therefore, for the TAP- $\alpha-Al_2O_3$  composite film,  $\tau_1 = 0.67$  ms was attributed to the  $Tb^{3+}$  centers in the TAP and  $\alpha-Al_2O_3$  phases and  $\tau_2 = 1.46$  ms corresponded to the  $Tb^{3+}$  center in the  $\alpha-Al_2O_3$  phase. For the TAG- $\alpha-Al_2O_3$  composite film,  $\tau_1 = 0.75$  ms was attributed to the  $Tb^{3+}$  center in the  $\alpha-Al_2O_3$  phase and  $\tau_2 = 1.31$  ms arose from the  $Tb^{3+}$  centers in the  $\alpha-Al_2O_3$  and TAG phases.

#### 4. Conclusions

We successfully synthesized TAP- $\alpha-Al_2O_3$  and TAG- $\alpha-Al_2O_3$  composite films by the LCVD method. The composite films had the lamellar structure at compositions close to the eutectic point, whereas the films showed the rod-like structure at compositions far from the eutectic point. The PLE peaks were associated with the transition of  $4f^75d$  to  $4f^8$  levels of the  $Tb^{3+}$  centers, and the emissions were associated with the transition of  $^5D_4$  to  $^7F_n$  ( $n = 3–6$ ) levels of the  $Tb^{3+}$  centers. The decay time constants of the TAP- $\alpha-Al_2O_3$  films were 0.67 and 1.46 ms, and those of the TAG- $\alpha-Al_2O_3$  films were 0.75 and 1.31 ms. Those values were attributed to the  $Tb^{3+}$  centers in the TAP, TAG, and  $\alpha-Al_2O_3$  phases.

#### Acknowledgments

This study was supported in part by JSPS KAKENHI Grant Numbers 21H05199, 24K91211, 24K21685, 24K21746, and 25H00796.

## References

- 1 Y. Waku, N. Nakagawa, T. Wakamoto, H. Ohtsubo, K. Shimizu, and Y. Kohtoku: *Nature* **389** (1997) 49. <https://doi.org/10.1038/37937>
- 2 Y. Waku, N. Nakagawa, T. Wakamoto, H. Ohtsubo, K. Shimizu, and Y. Kohtoku: *J. Mater. Sci.* **33** (1998) 4943. <https://doi.org/10.1023/A:1004486303958>
- 3 Y. Waku, N. Nakagawa, H. Ohtsubo, A. Mitani, and K. Shimizu: *J. Mater. Sci.* **36** (2001) 1585. <https://doi.org/10.1023/A:1017519113164>
- 4 A. Yoshikawa, K. Hasegawa, J. H. Lee, S. D. Durbin, B. M. Epelbaum, D. H. Yoon, T. Fukuda, and Y. Waku: *J. Cryst. Growth* **218** (2000) 67. [https://doi.org/10.1016/S0022-0248\(00\)00516-9](https://doi.org/10.1016/S0022-0248(00)00516-9)
- 5 E. Mihóková, M. Nikl, J. A. Mareš, A. Beitlerová, A. Vedda, K. Nejezchleb, K. Blažek, and C. D'Ambrosio: *J. Lumin.* **126** (2007) 77. <https://doi.org/10.1016/j.jlumin.2006.05.004>
- 6 Q. Sai, Z. Zhao, C. Xia, X. Xu, F. Wu, J. Di, and L. Wang: *Opt. Mater.* **35** (2013) 2155. <https://doi.org/10.1016/j.optmat.2013.05.035>
- 7 A. Shakhno, T. Zorenko, S. Witkiewicz-Łukaszek, M. Cieszko, Z. Szczepański, O. Vovk, S. Nizhankovskyi, Y. Siryk, and Y. Zorenko: *Materials* **16** (2023) 2701. <https://doi.org/10.3390/ma16072701>
- 8 Y. Ohashi, N. Yasui, Y. Yokota, A. Yoshikawa, and T. Den: *Appl. Phys. Lett.* **102** (2013) 051907. <https://doi.org/10.1063/1.4790295>
- 9 A. Yoshikawa, K. Kamada, S. Kurosawa, Y. Yokota, A. Yamaji, V. I. Chani, Y. Ohashi, and M. Yoshino: *J. Cryst. Growth* **498** (2018) 170. <https://doi.org/10.1016/j.jcrysgro.2018.02.032>
- 10 K. Kamada, H. Yamaguchi, N. Yasui, R. Ohashi, T. Den, K. J. Kim, M. Yoshino, A. Yamaji, S. Kurosawa, Y. Shoji, Y. Yokota, Vladimir. V. Kochurikhin, and A. Yoshikawa: *Jpn. J. Appl. Phys.* **60** (2021) SBBK04. <https://doi.org/10.35848/1347-4065/abd708>
- 11 C. He, Q. Sai, C. Xia, and H. Hu: *Cryst. Res. Technol.* **52** (2017) 1700056. <https://doi.org/10.1002/crat.201700056>
- 12 C. Deng, C. He, Q. Sai, Y. Liu, C. Xia, and X. Gu: *Optik* **160** (2018) 176. <https://doi.org/10.1016/j.ijleo.2018.01.093>
- 13 L. Sun, C. Zhou, T. Du, Z. Wu, Y. Lei, J. Li, H. Su, and J. Wang: *J. Inorg. Mater.* **36** (2021) 652. <https://doi.org/10.15541/jim20200508>
- 14 H. Su, J. Zhang, C. Cui, L. Liu, and H. Fu: *J. Alloys Compd.* **456** (2008) 518. <https://doi.org/10.1016/j.jallcom.2007.04.026>
- 15 J. Zhang, H. Su, B. Tang, L. Liu, and H. Fu: *J. Cryst. Growth* **310** (2008) 490. <https://doi.org/10.1016/j.jcrysgro.2007.10.054>
- 16 A. Ito, Y. You, T. Ichikawa, K. Tsuda, and T. Goto: *J. Eur. Ceram. Soc.* **34** (2014) 155. <https://doi.org/10.1016/j.jeurceramsoc.2013.07.025>
- 17 S. Matsumoto and A. Ito: *J. Ceram. Soc. Jpn.* **129** (2021) 1. <https://doi.org/10.2109/jcersj2.20156>
- 18 Y. Mitsuhashi, S. Matsumoto, and A. Ito: *J. Am. Ceram. Soc.* **106** (2023) 5140. <https://doi.org/10.1111/jace.19176>
- 19 S. Matsumoto, S. Kurosawa, D. Yokoe, T. Kimura, and A. Ito: *Opt. Mater.* **138** (2023) 113674. <https://doi.org/10.1016/j.optmat.2023.113674>
- 20 S. Matsumoto, A. Minamino, and A. Ito: *Sens. Mater.* **33** (2021) 2209. <https://doi.org/10.18494/SAM.2021.3325>
- 21 A. Ito, H. Kadokura, T. Kimura, and T. Goto: *J. Alloys Compd.* **489** (2010) 469. <https://doi.org/10.1016/j.jallcom.2009.09.088>
- 22 Y. Onishi, T. Nakamura, H. Sone, and S. Adachi: *Jpn. J. Appl. Phys.* **57** (2018) 082601. <https://doi.org/10.7567/JJAP.57.082601>
- 23 Y. Onishi, T. Nakamura, and S. Adachi: *J. Lumin.* **183** (2017) 193. <https://doi.org/10.1016/j.jlumin.2016.11.035>
- 24 Y. Onishi, T. Nakamura, and S. Adachi: *Jpn. J. Appl. Phys.* **55** (2016) 112401. <https://doi.org/10.7567/JJAP.55.112401>
- 25 Yu. V. Zorenko and V. I. Gorbenko: *Phys. Solid State* **51** (2009) 1800. <https://doi.org/10.1134/S1063783409090078>
- 26 Y. Hashimoto and A. Ito: *Mater. Lett.* **366** (2024) 136558. <https://doi.org/10.1016/j.matlet.2024.136558>
- 27 D. Nakauchi, T. Kato, N. Kawaguchi, and T. Yanagida: *Sens. Mater.* **33** (2021) 2203. <https://doi.org/10.18494/SAM.2021.3323>
- 28 M. Wojdyr: *J. Appl. Crystallogr.* **43** (2010) 1126. <https://doi.org/10.1107/S0021889810030499>